RSC Advances

PAPER

View Article Online
View Journal | View Issue

Cite this: *RSC Adv.*, 2020, **10**, 923

Raman spectroscopy and laser-induced degradation of groutellite and ramsdellite, two cathode materials of technological interest†

Simone Bernardini, *[a] Fabio Bellatreccia,[a] Giancarlo Della Ventura,[a] Paolo Ballirano[b] and Armida Sodo[a]

Received 22nd October 2019
Accepted 14th December 2019

DOI: 10.1039/c9ra08662e

rsc.li/rsc-advances

Manganese oxides are important geomaterials, used in a large number of applications. For instance, as pigments in art works or in the treatment and removal of heavy metals from drinking water. Particularly, ramsdellite [$Mn^{4+}O_2$] and groutellite [$(Mn_{0.5}{}^{4+},Mn_{0.5}{}^{3+})O_{1.5}(OH)_{0.5}$], because of their 2 × 1 frameworks that enable proton diffusion, are very important cathode materials. Manganese oxides commonly occur as crypto-crystalline and very fine mixtures of different Mn-phases, iron oxides, silicates and carbonates. Thus, proper characterization can be a difficult task using XRPD. The lack of Raman data on groutellite and the little and conflicting data on ramsdellite do not allow their proper identification by Raman spectroscopy. In this work we characterize natural mixtures of ramsdellite and groutellite by combining SEM-EDS, XRPD, FT-IR and Raman spectroscopy, to provide reference Raman spectra. Our data show that they have a typical and unmistakable spectra, allowing clear recognition. Moreover, we have investigated their laser-induced degradation. Our data show that groutellite transforms into ramsdellite, by the loss of H^+ and the oxidation of Mn^{3+} to Mn^{4+}, already at a very low laser power. Further increasing the laser power the formation of hausmannite [$Mn^{2+}Mn_2{}^{3+}O_4$] occurs *via* the reduction of Mn cations. Our data can be used to study the discharge mechanism in cathodic battery materials, by monitoring the Mn reduction from ramsdellite to groutellite, and finally to groutite [α-$Mn^{3+}OOH$]. Moreover, Raman mapping allows the study of their distribution in all the investigated samples and, indirectly, those of H^+ and Mn^{3+}, which plays a key-role in electrochemical activity of these compounds.

Introduction

Manganese oxides/hydroxides (MnOx) are important geomaterials, widespread in all geological environments. They result from the linkage of MnO_6 octahedra to form tunnel or layer frameworks[1] and typically occur as disordered, quasi-amorphous or cryptocrystalline phases, commonly intimately intermixed with other minerals such as iron oxides, carbonates and silicates.

MnOx have been used in various applications, including pigments in art works[2,3] or in environmental remediation to control the solubility and mobility of heavy metals in aqueous systems. Because of their high specific surface area[4] and their low point of zero charge[4,5] they may develop high absorption capacity with respect to arsenic and other potentially toxic elements.[6,7] The formation and distribution of MnOx are strongly controlled by fluid conditions (*e.g.* pH, Eh, ionic strength) as well as by microbial activity,[8–10] making them powerful paleo-environmental indicators.

The poor crystallinity of MnOx and their grain size, commonly in the nanoscale, makes their identification a real challenge using standard methods, such as X-ray diffraction. In contrast spectroscopic techniques, being sensitive to short-range arrangements between cations and anions, are particularly suitable to characterize these disordered materials. FT-IR is a well-recognized tool for their investigation,[11] although some MnOx show very similar absorption spectra that do not allow a definitive identification of the examined sample. Raman spectroscopy is better suited to study these materials, although data available in the literature are often conflicting, due to many factors such as the experimental condition, the incorrect identification of the examined material, and the presence of mixtures of different MnOx. An extremely important issue is in addition their high sensitivity to the laser heating; it has been shown that the interaction between the laser beam and the sample may easily lead to the degradation of the material as a function of the laser power and irradiation time.[12,13]

We published recently a detailed study of a large set of well-characterized MnOx minerals,[14] where these problems have

[a]*Dipartimento di Scienze, Università Roma Tre, Viale G. Marconi 446, 00146, Rome, Italy. E-mail: simone.bernardini@uniroma3.it*

[b]*Dipartimento di Scienze della Terra, Sapienza Università di Roma, P. le A. Moro 5, 00185, Rome, Italy*

† Electronic supplementary information (ESI) available: SEM-EDS, XRPD, FT-IR and Raman spectroscopy data. See DOI: 10.1039/c9ra08662e

been addressed and discussed. This work has been aimed at providing a references database of spectra to facilitate the application of Raman spectroscopy in the study of these materials. During this still ongoing work, we found samples of two extremely rare and poorly studied species: ramsdellite [$Mn^{4+}O_2$] and groutellite [$(Mn_{0.5}{}^{4+},Mn_{0.5}{}^{3+})O_{1.5}(OH)_{0.5}$]. No Raman data are available in the literature for groutellite, while those of ramsdellite are provided by,[15,16] who did not consider in his work the low thermal stability of the sample under the laser beam; we will show below that this is a critical aspect in the analysis of this mineral.

Ramsdellite usually occurs associated with pyrolusite [β-$Mn^{4+}O_2$] in low temperature hydrothermal deposits.[1] The first description of a synthetic compound corresponding to groutellite, and obtained as an intermediate product during the reduction of ramsdellite to groutite [α-MnOOH], was given by ref. 17. The occurrence in nature of groutellite, intermixed with ramsdellite, was later reported by ref. 18–20. However, to date groutellite has not been approved as a mineral species by the International Mineralogical Association (IMA).

Ramsdellite and groutellite are structurally closely related; they both have an orthorhombic *Pnma* symmetry,[21] and their structures consist of double chains (Fig. 1A) of nearly regular edge-shared MnO_6 octahedra, which link corners such as to form a 2 × 1 tunnels framework (Fig. 1B). In ramsdellite, Mn occurs exclusively as Mn^{4+} with an average ⟨Mn–O⟩ distance of 1.898 Å,[22] whereas in groutellite, half of the O^{2-} are replaced by OH^- groups located within the tunnels; the entry of the OH groups is balanced *via* the substitution of an equal amount of Mn^{3+} for Mn^{4+} in the metal framework. Due to Jahn–Teller distortion of Mn^{3+} occupied octahedra, in groutellite the ⟨Mn–O⟩ distances range between 1.87 and 2.13 Å.[22]

Ramsdellite, groutellite and nsutite [γ-MnO_2] and its synthetic analogue EMD (electrolytic Mn dioxide), a defects intergrowth of ramsdellite and pyrolusite domains,[23] are very important materials for electrochemical applications.[20,24–28] As a matter of fact, the multiple oxidation state of Mn and the presence in the structure of 2 × 1 tunnels (Fig. 1B) enable a rapid solid-state diffusion of protons, thus making these compounds important cathode materials.[29]

Groutellite is typically formed in cathodic battery materials because of the $Mn^{4+} \rightarrow Mn^{3+}$ reaction that is balanced by the incorporation of H within the tunnels.[29] Ramsdellite has a very low activation barrier for proton diffusion, which occurs by a rotation-and-jump mechanism along the 2 × 1 open tunnels.[29] Twinning and other defects can have a large adverse effect on the proton diffusivity. The activation energy in the reduced phase is higher due to structural changes induced by Jahn–Teller distortions and consequent interaction between the H atoms.[29]

As mentioned above, MnOx have a high sensitivity to the laser beam, therefore, a proper characterization of the laser-induced degradation of the different Mn-species is highly desirable for using Raman spectroscopy as a tool for their study. The blackish MnOx strongly absorb the photon energy, producing a local heating that may cause shifts and broadening of the Raman peaks due to photo- and/or thermal-induced chemical reactions. This effect may thus lead to significant misleading for the identification of the examined sample.

The thermal behaviour of MnOx has been widely investigated by thermogravimetric analysis and X-ray diffraction, providing an improved understanding of the spectra and of the changes taking place during samples irradiation. Accordingly, the thermal stability of the samples has been shown to depend on the structural arrangement, the type of the tunnel/layer cations or molecules, the grain size, and the crystallinity.[30–32] In addition to these, the boundary conditions (oxidation environment, humidity, time duration *etc.*) also during the analysis may play an important role.[33] According to some authors[22] groutellite completely transforms into ramsdellite when heated between 530 and 600 K. During the transformation the unit-cell volume decreases by ~7%, due to the oxidation of Mn^{3+} to the smaller Mn^{4+}. High-temperature IR spectroscopy shows the disappearance of the OH band at ~3400 cm^{-1} due to the loss of H^+ as Mn is oxidized during the experiment. Due to the Jahn–Teller octahedral distortion of Mn^{3+} there is an axial elongation of the MnO_6 octahedra in groutellite plus a slight octahedral rotation.[22] Above 600 K ramsdellite starts transforming into pyrolusite. Pyrolusite is also very sensitive to the heating and, at ~725 K, transforms into bixbyite. For further *T* increase up to ~1300 K the formation of hausmannite is finally observed.[31,34]

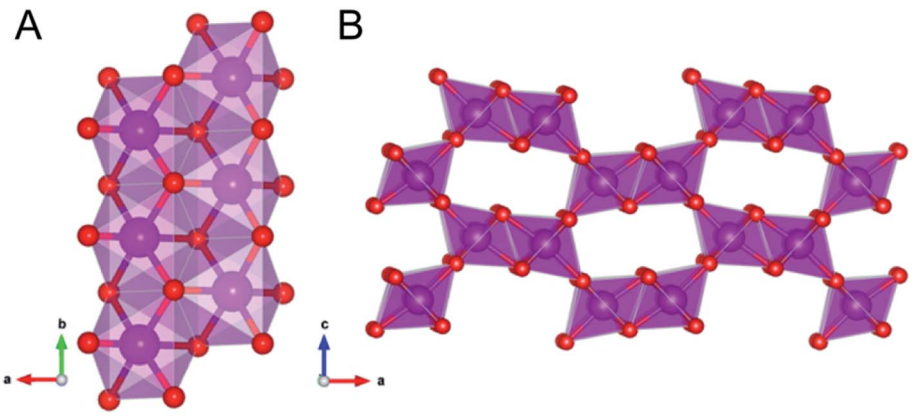

Fig. 1 The linkage within the Mn double-chains (A). Polyhedral representation of the ramsdellite structure showing the 2 × 1 tunnels (B).

These phase transformations may occur due to the laser irradiation during the Raman analysis and could thus lead to mistakes for the identification of the sample; such a problem can be easily avoided by carefully cheeking for the appearance in the spectra of those peaks due to the high temperature phases, such as pyrolusite, bixbyite and hausmannite, that are available in the literature.[14,35]

To date the lack of Raman data for groutellite and the few and conflicting data for ramsdellite prevent their identification by Raman spectroscopy. The final goal of this work is at providing reference Raman spectra, acquired on previously well-characterized samples. A second, important aspect addressed in this work is the characterization of their degradation behaviour during sample irradiation, an issue that is fundamental to assess the application of Raman spectroscopy in the study of these important cathode materials. For this purpose, very fine mixtures of groutellite and ramsdellite were characterized by combining X-ray powder diffraction (XRPD), scanning electron microscopy with energy-dispersive spectroscopy (SEM-EDS), and Fourier transform infrared (FT-IR) methods, before collecting the Raman patterns and studying their laser-induced degradation.

Samples and experimental methods

One sample from the Calabona Mine (Sardinia, Italy), and a second one from Chiaramonti (Sardinia, Italy), have been sampled from the specimens G5502 and G5695 belonging to the lito-mineralogical collection of the Natural History Museum – S.M.A. of the University of Florence. Both were carefully examined by optical microscopy and found to consist of sub-millimetric aggregates of light- or dark-gray phases. SEM-EDS analyses indicated a mixture of acicular or massive micrometric MnOx and quartz (Fig. S1A†) for sample G5502, and a massive aggregate of only MnOx for sample G5695 (Fig. S1B†). The studied material was thus purified by hand-picking and divided into two fractions: the first was ground and used for XRPD and FTIR; the second for Raman analyses.

SEM analyses were collected at the Interdepartmental Electron Microscopy Lab (LIME), Roma Tre University, using a Zeiss Sigma 300 FE-SEM (field-emission scanning electron microscope). The microscope is equipped with a HDBSE (high-resolution backscattered electron) detector and an energy dispersive (EDS) Bruker QUANTAX detector. The elemental composition was determined using an accelerating voltage of 20 kV, a filament current of 1.80 A and an aperture size of 20 μm.

Diffraction data were collected at the X-ray Powder Diffraction Laboratory, Department of Earth Sciences, Sapienza University of Roma, using a Bruker AXS D8 Advance operating in θ/θ geometry. Samples were prepared as capillaries. The instrument is fitted with an incident beam multilayer graded focussing (Göbel) mirror, radial Soller and a position sensitive VÅNTEC-1 detector. Patterns were measured in the 6–80° 2θ angular range, 0.022° 2θ step size, and 2 s counting time.

Powder FTIR spectra were collected at the Infrared Spectroscopy Laboratory, Department of Science, Roma Tre University, using a Nicolet iS50 FTIR spectrometer equipped with a DTGS detector and a KBr beamsplitter; the nominal resolution was 4 cm^{-1}, and 64 scans were averaged for each sample and for the background. Samples were prepared as pellets containing about 1 mg of powdered mineral in 200 mg of KBr.

Raman measurements were performed at the Raman Spectroscopy Laboratory, Department of Science, Roma Tre University, at room temperature using an inVia Renishaw Raman spectrometer equipped with a diode laser (532 nm, output power 50 mW), an edge filter to select the Raman scattering avoiding the elastic contribution, a 1800 lines per mm diffraction grating and a Peltier cooled 1024 × 256 pixel CCD detector. Samples were mounted on the manual stage of a Leica DM2700 M confocal microscope. Focusing of the laser beam and collection of Raman signals was realised by a 50× long-working distance objective. The spectra were recorded using a controlled laser power, the details will be reported in the Results and discussion section. The Raman spectrometer was calibrated prior to the measurements using a Si wafer and by performing the automatic offset correction. The spectra acquisition and data analyses were accomplished using WiRE™ and Origin software. The peak positions are estimated to be accurate to at least ±2 cm^{-1}.

For each sample, we collected several point analyses in order to check for inhomogeneities. After selecting the point locations for ramsdellite and groutellite, respectively (see text) we performed measurements by increasing the laser power in order to follow the degradation of the phase and the evolution of the scattered signal.

Experimental results

X-ray powder diffraction data showed very sharp peaks (Fig. S2†), suggesting both samples to consist of mixtures of well-crystallized Mn-phases; the identification of the different species was based on the PDF (Powder Diffraction File). Inspection of Fig. S2† shows that sample G5695 consists of ramsdellite, recognized *via* Bragg peaks at *d*-spacing (Å)(*hkl*) 4.06(101), 2.44(210), 2.55(301) (PDF number 00-043-1455), with minor groutellite, with peaks at 4.22(101), 2.63(301), 2.37(111) (PDF number 00-012-0720) and pyrolusite, with peaks at 3.11(110), 2.41(101), 1.62(211) (PDF number 00-024-0735). Sample G5502 consists of abundant groutellite, together with ramsdellite and pyrolusite; traces of quartz were also identified (Fig. S2†).

FT-IR spectra collected on the same powders previously used for XRD data collection are also given in Fig. S3.† The spectra collected on both samples G5695 and G5502 show absorption bands at ∼414, 485, 525, 555, 649, 690, 761, 3390 cm^{-1} and shoulders at ∼599 and 792 cm^{-1} (Fig. S3†). All these bands belong to groutellite,[36] in particular the sharp peak at 3393 cm^{-1} that can be assigned to the OH-stretching mode. Moreover, bands at 485, 525, 555 and 761 cm^{-1} and shoulders at ∼599 cm^{-1} also belong to ramsdellite.[36] The less abundant pyrolusite, detected by X-ray diffraction, showing strong absorption bands in the same spectral range of groutellite and ramsdellite, between 535 and 615 cm^{-1},[11] cannot be recognized in our samples by FT-IR.

Raman spectroscopy

Based on preliminary XRD and FT-IR data, Raman spectra were collected on several points of sample G5502, consisting of abundant groutellite, plus weak amounts of ramsdellite and pyrolusite, at a very low laser power (1.15 mW) in order to avoid any possible samples degradation.

Three types of spectra with different features were obtained on different sample locations: (1) a spectrum (Fig. S4†) with an intense peak at 660 cm^{-1} and weak peaks at 533 and 755 cm^{-1}; based on literature data[14] this pattern can be assigned to the trace amounts of pyrolusite in the mixture. (2) A spectrum with sharp and relatively strong bands at 270, 486, 525, 578 and 650 cm^{-1}, plus a weak band at 745 cm^{-1} and a shoulder at 632 cm^{-1} (Fig. 2A(b)). (3) A third type of spectrum with a strong band at ~648 cm^{-1} with a very weak band at 525 cm^{-1} and a weak shoulder at ~743 cm^{-1} (Fig. 2B(b)); it is notable that, at this sample location, an unresolved and very noisy pattern was obtained at 0.18 mW (Fig. 2B(a)), while defined Raman scatterings could be obtained at 1.15 mW. Although patterns 2 and 3 show bands in the range typical of MnOx they do not match any spectrum reported in the literature for these compounds.[14] However, based on the XRD data discussed above, we can infer these patterns to be related to groutellite and ramsdellite, finely intermixed with pyrolusite in the studied sample.

To support this hypothesis and assign correctly each pattern to the corresponding phase, we performed heating experiments on the studied samples. As discussed above, when heated between 530 and 600 K groutellite transforms completely into ramsdellite[11] therefore we heated sample G5502 from room temperature up to 600 K in 30 minutes and let it cool down just removing it from the furnace (sample G5502_600 K). In the same way, sample G5502_673 K was obtained by heating the powder from RT up to 673 K, *i.e.* above the stability limit of ramsdellite, in 30 min, and holding it at this temperature for 10 min before cooling. X-ray diffraction showed, for sample G5502_600 K, the complete disappearance of the groutellite peaks and the presence of ramsdellite, pyrolusite and traces of quartz (Fig. S2†). The FT-IR pattern showed all bands of ramsdellite at 482, 530, 694 and shoulders at 555, 610, 759 cm^{-1}.[36] The disappearance of the OH peak at 3393 cm^{-1} (Fig. S3†) confirmed the complete transformation of groutellite into ramsdellite. Finally, XRPD showed the sample treated at 673 K to consist of almost monophase pyrolusite with traces of ramsdellite and quartz (Fig. S2†). The FT-IR pattern showed only bands of pyrolusite at 400, 472, 563 and 686 cm^{-1} and shoulders at 530 and 619 cm^{-1} (Fig. S3†).[11]

Raman spectra collected on sample G5502_600 K (Fig. 3a) show a strong band at ~649 cm^{-1} and weak bands at ~526 and 576 cm^{-1}, with weak components at 270 and 491 cm^{-1}. On the other side, all Raman spectra collected on sample G5502_673 K show a strong band at ~650 cm^{-1} and weak components at ~528, 360 and 310 cm^{-1} (Fig. 3b). By comparing the results from Fig. 2A(b), B(b) and 3 and considering the information from X-ray diffraction and FT-IR we can now assign the spectrum given in Fig. 2A(b) to groutellite and the spectrum in Fig. 2B(b) to ramsdellite; the minor peaks at 270, 491 and 576 cm^{-1}, detected in sample G5502_600 K (Fig. 3a), can thus be

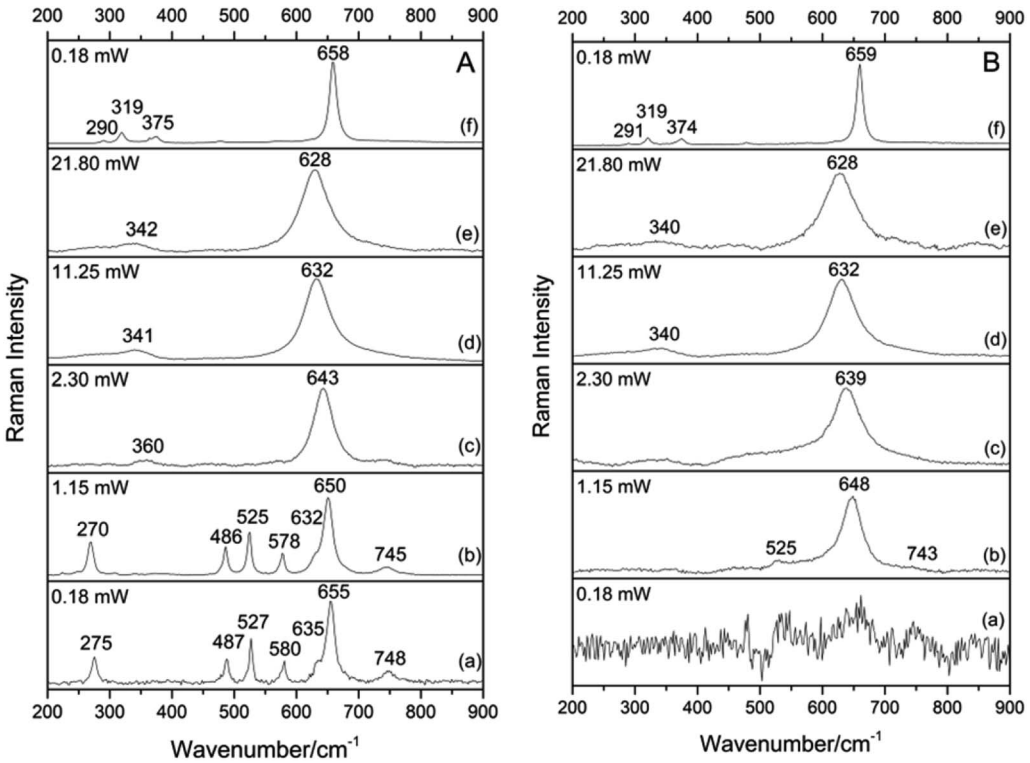

Fig. 2 Evolution of the Raman spectra of sample G5502 collected by increasing the laser power. (A) groutellite (B) ramsdellite. Spectra collected at $\lambda = 532$ nm.

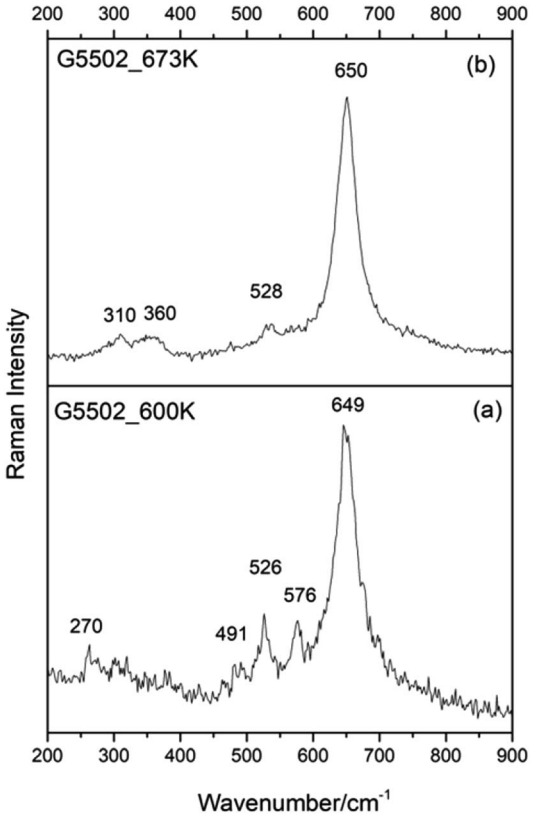

Fig. 3 Selected Raman spectra collected for sample G5502 heated at 600 K (a) and 673 K (b). Spectra collected at $\lambda = 532$ nm, laser power 1.15 mW.

assigned to trace amount of groutellite in the sample, not detected by X-ray diffraction. In agreement with this inference these peaks disappear when the sample is heated to 673 K, a condition where all groutellite is transformed to ramsdellite. Our spectra assignment is further confirmed by the Raman spectra collected on sample G5695, which show the same features recognized in the spectra collected on sample G5502.

Our data for ramsdellite are in good agreement with those reported in the RRUFF database, ID R050552, where bands at 528, 649 and 753 cm^{-1}, are given. While are in strong disagreement with the data obtained by ref. 15, which report bands at 143, 294, 518, 580, 630, 680 and 740 cm^{-1}. Moreover, our data are in disagreement with those obtained by ref. 16, which report bands at 275, 387, 490, 522, 575, 630, 648 and 742 cm^{-1}. It should be noted that these spectral features are quite similar to those of our groutellite, possibly because the sample studied was a fine-grained mixtures of different MnOx phases.

The laser-induced degradation of groutellite and ramsdellite

As already discussed in the introduction, groutellite and ramsdellite are extremely sensitive to temperature. Besides any consideration on their stability for geological or technological purposes, this feature may generate misinterpretations when applying Raman spectroscopy to their investigation. According to the literature[22] groutellite transforms into ramsdellite at T as low as ~530 K; for further temperature increase there is the formation of pyrolusite ($Mn^{4+}O_2$) at ~600 K, bixbyite ($Mn_2^{3+}O_3$) at ~725 K and finally hausmannite ($Mn^{2+}Mn_2^{3+}O_4$) at ~1300 K. To check for the transformation of the samples due to the laser heating, we collected several spectra using different laser power to monitor the laser-induced degradation of our MnOx.

Groutellite

We started our experiments on the more heat-sensitive groutellite (Fig. 2A). At 0.18 mW the spectrum is already well defined (Fig. 2A(a)), and from 0.18 mW up to 1.15 mW there is no change in the scattering, except a slight peak shift (~3 cm^{-1}) toward lower wavenumbers for all bands (Fig. 2A(b)). At 2.30 mW there is a strong change in the spectrum: only the intense band originally at ~650 cm^{-1}, now shifted to 643 cm^{-1}, is recognized, plus a weak and broad component at ~360 cm^{-1} (Fig. 2A(c)). Based on the above data, therefore, at this laser-power there is the complete transformation of groutellite into ramsdellite due to the laser-induced heating. In other words, for a laser power > 2.30 mW there is the oxidation of Mn^{3+} to Mn^{4+} coupled to a loss of hydrogen from the structure, analogous of what observed during the heating experiments described above. Therefore, Raman spectra of ramsdellite produced by laser-degradation of groutellite differ from those collected on the untreated material only for the presence of a weak and broad band at ~360 cm^{-1}. As already discussed, also the spectra of ramsdellite annealed after heating the sample in the furnace show these features. These bands, occurring in the region of the skeletal vibrations (200–450 cm^{-1}),[16] could be assigned to the not yet suppressed octahedral rotation due to the $Mn^{4+} \rightarrow Mn^{3+}$ substitution during the groutellite to ramsdellite transformation. According to the structural data found in the literature[22] groutellite, compared to ramsdellite, shows an axial elongation of the Mn–O octahedra and a slight octahedral rotation due to the Jahn–Teller axial distortion on the $Mn^{3+}O_6$ octahedra. In addition, structural defects could locally lead to a variation of the average symmetry. Further increasing the laser power to 21.80 mW the 643 cm^{-1} bands shifts to 628 cm^{-1} while the 360 cm^{-1} component shifts to 342 cm^{-1} (Fig. 2A(e)). This spectrum is very similar to those obtained by using a high laser power on pyrolusite and manganosite;[14,35] other authors assigned it to an "unknown material X", a not yet identified MnOx phase.[35] Finally, the spectrum collected after decreasing the laser power to 0.18 mW shows a sharp band at 658 cm^{-1} and weak peaks at 290, 319 and 375 cm^{-1} (Fig. 2A(f)), a spectrum characteristic of hausmannite.[14,37] The series of spectra given in Fig. 2A provides also a further confirmation to the proposed band assignment discussed on the heated samples. As a matter, with the laser heating we reproduce the same kind of reaction transforming groutellite into ramsdellite.

Ramsdellite

At a laser power of 0.18 mW no Raman scattering is observed for ramsdellite (Fig. 2B(a)), while at a laser power of 1.15 mW a strong band at 648 cm^{-1} and a very weak band at 525 and a weak shoulder at ~743 cm^{-1} show up (Fig. 2B(b)). At 2.30 mW the strong band shift to 639 cm^{-1} and the weak bands disappear (Fig. 2B(c)). Increasing the laser power up to 21.80 mW this

band shift further, up to 628 cm^{-1}, while a broad and weak band at 340 cm^{-1} shows up (Fig. 2B(e)). Therefore, at high laser power also ramsdellite transform into the "unknown material X", as already observed for groutellite (this work) and for pyrolusite and manganosite.[14,35] Finally, as already observed for groutellite, after decreasing the laser power to 0.18 mW the spectrum shows a very strong and sharp band at 659 cm^{-1} and weak bands at 291, 319 and 374 cm^{-1} of hausmannite (Fig. 2B(f)).

In synthesis, starting from groutellite the laser heating leads to the oxidation of Mn whereby ramsdellite is formed by loss of H^+ and the oxidation of Mn^{3+} to Mn^{4+}. For further increase of the laser power the final formation of hausmannite is observed (Fig. 2); this observation implies the reduction of Mn^{4+} to $Mn^{3+/2+}$ and the rearrangement of the structure in a distorted spinel framework.

Mapping of groutellite/ramsdellite intergrowths

The definition of the Raman spectra of groutellite and ramsdellite may be used to study the spatial distribution between these phases in a sample. For this purpose, a grid of single-point spectra was collected for specimen G5502 at 1.0 μm step for a total number of 156 points, from 499 cm^{-1} to 700 cm^{-1}. A laser power of 1.15 mW and an exposure time of 5 s was used in order to avoid any possible degradation of the sample. The intensity ratio between the band at 580 cm^{-1}, that is a unique feature of groutellite, and the band at 650 cm^{-1}, belonging to both Mn-phases, was integrated over the scanned area. The resulting image (Fig. 4) shows that sample G5502 indeed consists of a micron-scale intergrowth of groutellite and ramsdellite. In more detail, inspection of Fig. 4 shows micrometric, almost rounded ramsdellite crystallites (red to black in Fig. 4) dispersed within a groutellite matrix (white and yellow areas). We stress here that the zoning of groutellite corresponds indirectly to the distribution of H^+ and/or Mn^{3+} in across the sample, therefore the maps like those displayed in Fig. 4 indeed provide the distribution of hydrogen and of the different oxidation state of Mn across the sample. Besides the evident bearing for geological/environmental applications, this method has also interesting applications for the study of technologically relevant materials. As discussed above, ramsdellite and groutellite are part of a reaction series of the electrochemical process during a battery operation. Our work shows that Raman imaging may provide the possibility to monitor, at a very fine spatial resolution (<1 μm) the reaction products and development. The Raman spectrum of groutite, that is the final product of the discharge of alkali batteries is known in the literature[16,35] therefore, by Raman spectroscopy it is possible to monitor the entire electrochemical process by considering that the first step, *i.e.* the reduction of ramsdellite to groutellite can be checked by the appearance in the spectrum of a peak at ~580 cm^{-1}, while the transformation of groutellite into groutite can be checked by the appearance of a band at ~552 cm^{-1}.[16,35]

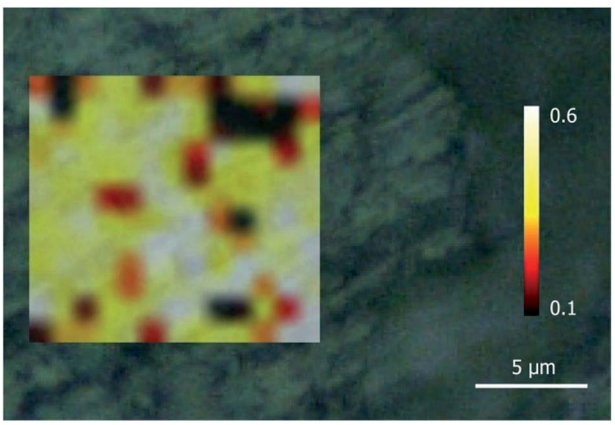

Fig. 4 Map resulting from the integration of the intensity ratio between band at 580 and 650 cm^{-1} in the groutellite–ramsdellite intergrowth. High band ratio (white/yellow colour) maps the distribution of groutellite (or, indirectly, H^+ and/or Mn^{3+}), while low band ratio (red/black dots) that of ramsdellite.

Conclusions

In this work we provide the Raman spectra of groutellite and ramsdellite, collected on two well-characterized natural mixtures samples by using a combination of SEM-EDS, XRPD, FT-IR and Raman spectroscopy. In addition we closely examined the degradation of these Mn-compounds, induced by increasing laser power during the Raman analysis.

Our results show that the Raman spectrum of ramsdellite exhibits a strong band at ~650 cm^{-1} and a weak band at ~525 cm^{-1} and a very weak shoulder at ~743 cm^{-1}. The spectrum of groutellite shows an intense peak at ~650 cm^{-1} plus weak bands at ~275, 487, 527, 578, 755 and a shoulder at ~630 cm^{-1}.

The degradation of groutellite leads to the formation of ramsdellite, already at a very low laser power. For further increase of the laser power the formation of hausmannite is observed.

Because of their 2 × 1 structural framework, which enables protons diffusion, groutellite and ramsdellite are very important cathode materials. During the discharge mechanism in alkaline cell Zn is oxidized at the anode, while protons are diffused into the MnO_2 (ramsdellite structure) constituting the cathode. As a consequence of this process, ramsdellite transforms into groutellite and finally into groutite $Mn^{3+}O(OH)$.[29] Our results show that Raman spectroscopy can be a powerful tool to monitoring these processes at a very fine scale when using Raman mapping.

Groutellite and ramsdellite are almost identical from a structural point of view, and differ only for the presence/absence of H^+ in the structural tunnels and for the average oxidation state of Mn. Therefore, these phases cannot be differentiated by SEM-EDS; FTIR spectroscopy in the OH-stretching region could be effective because of the presence of hydrogen in groutellite, however the technique is unable to resolve groutellite/ramsdellite intergrowth at a fine scale.

Conflicts of interest

There are no conflicts to declare.

Acknowledgements

Thanks are due to Dr Vanni Moggi Cecchi, Curator of the Lito-Mineralogical collection of the Natural History Museum – Sistema Museale di Ateneo of the Università degli Studi di Firenze, for kindly providing the studied samples and for his assistance during samples selection. The Grant to Department of Science, Roma Tre University (MIUR-Italy Dipartimenti di Eccellenza, ARTICOLO 1, COMMI 314–337 LEGGE 232/2016) is gratefully acknowledged.

References

1 J. E. Post, *Proc. Natl. Acad. Sci. U. S. A.*, 1999, **96**, 3447.
2 P. Jezequel, G. Wille, C. Beny, F. Delorme, V. Jean-Prost, R. Cottier, J. Breton, F. Dure and J. Despriee, *J. Archaeol. Sci.*, 2011, **38**, 1165.
3 M. C. Caggiani and P. Colomban, *J. Raman Spectrosc.*, 2011, **42**, 839.
4 R. M. McKenzie, *Aust. J. Soil Res.*, 1981, **19**, 41.
5 D. W. Oscarson, P. M. Huang, W. K. Liaw and U. T. Hammer, *Soil Sci. Soc. Am. J.*, 1983, **47**, 644.
6 B. J. Lafferty, M. Ginder-Vogel and D. L. Sparks, *Environ. Sci. Technol.*, 2010, **44**, 8460.
7 B. J. Lafferty, M. Ginder-Vogel and D. L. Sparks, *Environ. Sci. Technol.*, 2011, **45**, 9218.
8 B. M. Tebo, J. R. Bargar, B. G. Clement, G. J. Dick, K. J. Murray, D. Parker, R. Verity and S. M. Webb, *Annu. Rev. Earth Planet. Sci.*, 2004, **32**, 287.
9 K. M. Sutherland, S. D. Wankel and C. M. Hansel, *Geobiology*, 2018, **16**, 399.
10 X.-D. Jiang, X.-M. Sun and Y. Guan, *J. Asian Earth Sci.*, 2019, **171**, 46.
11 R. M. Potter and G. R. Rossman, *Am. Mineral.*, 1979, **64**, 1199.
12 E. Widjaja and J. T. Sampanthar, *Anal. Chim. Acta*, 2007, **585**, 241.
13 I. Rusakova, T. Ould-Ely, C. Hofmann, D. Prieto-Centuriòn, C. S. Levin, N. J. Halas, A. Luttge and K. H. Whitmire, *Chem. Mater.*, 2007, **19**, 1369.
14 S. Bernardini, F. Bellatreccia, A. Casanova Municchia, G. Della Ventura and A. Sodo, *J. Raman Spectrosc.*, 2019, **50**, 873.
15 C. Julien, M. Massot, S. Rangan, M. Lemal and D. Guyomard, *J. Raman Spectrosc.*, 2002, **33**, 223.
16 C. Julien, M. Massot and C. Poinsignon, *Spectrochim. Acta, Part A*, 2004, **60**, 689.
17 C. Klingsberg and R. Roy, *Am. Mineral.*, 1959, **44**, 819.
18 M. Fleischer, W. E. Richmond and H. T. Evans, *Am. Mineral.*, 1962, **47**, 47.
19 J. E. Post and D. R. Ross, *Eos*, 1989, **70**, 352.
20 L. A. H. MacLean, C. Poinsignon, J. M. Amarilla, F. Le Cras and P. Strobel, *J. Mater. Chem.*, 1995, **5**, 1183.
21 A. N. Byström, *Acta Chem. Scand.*, 1949, **3**, 163.
22 J. E. Post and P. J. Heaney, *Am. Mineral.*, 2004, **89**, 969.
23 S. Turner and P. Buseck, *Nature*, 1983, **304**, 143.
24 J. M. Amarilla, L. A. H. MacLean, F. Tedjar, F. Le Cras and C. Poinsignon, *Mater. Res. Soc. Symp. Proc.*, 1995, **369**, 87.
25 M. Manickam, P. Singh, T. B. Issa, S. Thurgate and R. De Marco, *J. Power Sources*, 2004, **130**, 254.
26 W. Bowden, T. Bofinger, F. Zhang, N. Iltchev, R. Sirotina, Y. Paik, H. Chen, C. Grey and S. Hackney, *J. Power Sources*, 2007, **165**, 609.
27 R. Ranjusha, T. S. Sonia, S. Roshny, V. Lakshmi, S. Kalluri, T. N. Kim, V. N. Shantikumar and A. Balakrishnan, *Mater. Res. Bull.*, 2015, **70**, 1.
28 I. Stoševski, A. Bonakdarpour, F. Cuadra and D. P. Wilkinson, *Chem. Commun.*, 2019, **55**, 2082.
29 D. Balachandran, D. Morgan and G. Ceder, *J. Solid State Chem.*, 2002, **166**, 91.
30 D. L. Bish and J. E. Post, *Am. Mineral.*, 1989, **74**, 177.
31 M. I. Zaki, M. A. Hasan, L. Pasupulety and K. Kumari, *Thermochim. Acta*, 1997, **303**, 171.
32 O. Ghodbane, J. L. Pascal, B. Fraisse and F. Favier, *ACS Appl. Mater. Interfaces*, 2010, **2**, 3493.
33 B. Liu, P. S. Thomas, A. S. Ray and R. P. Williams, *J. Therm. Anal. Calorim.*, 2004, **76**, 115.
34 J. L. Kulp and J. N. Perfetti, *Mineral. Mag.*, 1950, **29**, 239.
35 M. C. Bernard, A. Hugott-Le Goff, B. V. Thi and S. Cordoba de Torresi, *J. Electrochem. Soc.*, 1993, **140**, 3065.
36 N. V. Chukanov and A. D. Chervonnyi, *Infrared Spectroscopy of Minerals and Related Compounds*, Springer Mineralogy, Switzerland, 2016.
37 F. Buciuman, F. Patcas, R. Craciun and D. R. T. Zahn, *Phys. Chem. Chem. Phys.*, 1999, **1**, 185.